

# A method to measure the embedded crack length and position in high-density polyethylene using microseconds ultrasound time signal

Sijun Niu<sup>a</sup>, Venkatsai Bellala<sup>a,b</sup>, Daanish Aleem Qureshi<sup>a</sup>, Vikas Srivastava<sup>a,b,\*</sup>

<sup>a</sup>*School of Engineering, Brown University, 184 Hope Street, Providence, RI 02912, USA*

<sup>b</sup>*Center for Biomedical Engineering, Brown University, 184 Hope Street, Providence, RI 02912, USA*

---

## Abstract

High-density polyethylene (HDPE) is a semi-crystalline polymer used in several critical applications, ranging from cooling water pipelines in nuclear power plants and distribution pipelines for natural gas and hydrogen to biomedical implants. Embedded crack-like flaws form within HDPE during fabrication or operations. Non-visible flaws grow over time and can cause catastrophic failure if undetected. Large structures such as HDPE pipelines where the location of a flaw is not known require a fast, non-destructive evaluation (NDE) method where the sensor can move rapidly across the structure with very short microseconds at each location. This is only possible if the flaw is evaluated in HDPE and other polymeric structures using microseconds of time signal. Ultrasonic A-scan (time signal) allows for the rapid scan of large structures. We propose and show the accuracy of a machine learning-based Ultrasound NDE method that can rapidly and accurately predict embedded crack length and position simultaneously in HDPE with only tens of microseconds of time signal sensing. Current NDE methods rely on technical experts to evaluate the ultrasound measurements, which leads to high uncertainty and errors as the quantitative information about a crack is subtly encoded in the reflected signal. A method to quantify crack size in HDPE and other polymers using a very short Ultrasound time signal is lacking. We suggest that an optimally trained machine learning model can decipher the crack characteristics using short measures of time signal, but a lack of large, well-distributed, and labeled datasets to train machine learning models continues to be a major limitation. To overcome this limitation, we have conducted computer simulations of ultrasound on HDPE to develop training data. We show that fully finite element simulations trained convolutional neural network (CNN) can accurately predict crack lengths and positions in HDPE from experimentally measured ultrasound A-scan microsecond signals, with an average error of 3.2% for the crack lengths and 3.8% for the crack positions. Our method is based on the 1D time amplitude signal acquired over a very short time period and not based on 2D image analysis as the image rendering NDT is

---

\*Corresponding author

*Email address:* vikas\_srivastava@brown.edu (Vikas Srivastava)

very slow and susceptible to losing subtle but important crack feature information during the post-processing to create images. The proposed methodology presents a pathway for training CNN using computationally generated data and applying the trained CNN in the field to quantify hidden cracks in large HDPE or other polymer structures using ultrasound time signals when the measurement window is very small.

*Keywords:* High-Density Polyethylene, Ultrasound, Non-Destructive Evaluation, Finite Element Analysis, Convolutional Neural Network, Polymer NDT

---

## 1. Introduction

Polyethylene (PE) is a semi-crystalline polymer with repeating ethylene monomer units in the polymer chain. PE consists of a highly ordered and molecularly structured crystalline phase and an amorphous phase of entangled disordered chains. High-density polyethylene (HDPE) is a highly linear variant of PE as it lacks branches, enabling close packing of its polymer chains. Similar to PE, it is a low-cost thermoplastic polymer consisting of a mixed amorphous and crystalline structure and has high crystallinity, strength, and moderate stiffness. HDPE is used in various biomedical and industrial applications [1, 2]. Within the medical device space, HDPE is used for bone grafts, surgical implants, and total joint replacements [2, 3]. HDPE pipes are used for road drains [4, 5], and natural gas distribution pipes [6, 7, 8] due to their resistance to cracking and chemical interactions and because of their low cost and ease of installation [1]. HDPE has been utilized to transport cooling water in nuclear power plants [9]. HDPE, due to its chemical resistance to hydrogen, will play a crucial role in clean energy hydrogen storage and transport [10].

HDPE is easily recyclable [11], and has long-term durability and performance [12, 13, 11]. However, flaws introduced in manufacturing [14] and during operations can weaken the polymer structure, reducing its performance and life cycle. Extrusion defects were found to be responsible for the majority of crack initiations in HDPE tubes [15]. HDPE pipes in highway drainage systems showed significant internal cracks during operations [14], and HDPE pipe joints, such as those formed using butt-fusion, are prone to embedded defects [16]. Even under low stresses, HDPE is susceptible to slow crack growth [17]. Detection and characterization of cracks or crack-like flaws become essential to assess the long-term integrity of the HDPE structure. Crack length is the most important characteristic determining the load or stress under which an HDPE structure will fail. For a crack of length  $a$ , the crack tip opening displacement rate  $\dot{\delta}$  for a slowly growing crack in PE can be estimated using equation 1 [18]. Chan and Williams [19] experimentally demonstrated that linear elastic fracture mechanics can approximately describe the failure stress  $\sigma_f$  in PE, which indicates the relation shown in equation 2.

$$\dot{\delta} \propto a^m \quad \text{where } m > 0 \quad (\text{Slow Crack Growth Model}) \quad (1)$$

$$\sigma_f \propto a^m \quad \text{where } m = -\frac{1}{2} \quad (\text{Linear Elastic Fracture Mechanics}) \quad (2)$$

A variety of tests can be applied to assess the long-term health and performance of HDPE structures. Environmental stress crack resistance and time-temperature superposition test methods can estimate the chemical and mechanical/thermal degradation profile of HDPE specimens. However, these test methods are destructive and not very useful for in-field measurements [20]. Non-destructive testing (NDT) or non-destructive evaluation (NDE) allows the detection of previously unknown cracks and flaws without damaging the specimen. Visual and other surface examination techniques can identify surface damages [9] but are ineffective for embedded flaws. Infrared thermography tests for flaws in HDPE pipes and tanks by analyzing heat dissipation from damaged regions, but its accuracy is limited [21]. Microwave imaging has been shown to be capable of detecting internal flaws and voids in HDPE pipes [22, 23] but is limited by low resolution. Ultrasound is a promising NDE method. Ultrasound methods are frequently utilized to image and detect embedded cracks in HDPE [23, 24, 25, 26, 27]. An ultrasound device propagates waves through a specimen, and waves that reflect from an internal anomaly are analyzed to discern the anomaly. A common ultrasonic flaw detection approach is the pulse-echo technique: reflections of the generated wave from flaws and cracks are recorded as echoes or peaks in a scan. An A-scan is a simple time–amplitude ultrasound signal. B-scan, on the other hand, produces a 2D cross-sectional image of the anomaly from the reflected ultrasound signals. A B-scan requires significantly longer data collection time at a location and depends on the post-processing of raw data to create 2D images. *Compared to image based NDE methods, microseconds raw time signal sensing (A-scan) provides fast scanning essential for evaluating large structures. A time signal based NDE method is also not limited by approximation errors (loss of important information contained in very subtle signal variations that account for quantitative measures of the change in the size of the flaw) made by post-processing algorithms. In this paper, we show that the microseconds of the flaw-reflected ultrasound time signal for HDPE contain sufficient information to accurately quantify the length and position of an embedded non-visible crack.* Machine learning can be applied to interpret ultrasound signals to eliminate technician error [28]. Machine learning has been applied to measure embedded crack characteristics in steel from ultrasound measurements [29, 30]. Machine learning is used in fields ranging from computer vision and speech recognition [31] to problems in mechanics [32, 33, 34, 35, 36, 37, 38]. Convolutional neural networks (CNNs) have efficient pattern recognition, and image classification, especially when the dimensions of the raw inputs are very large and discerning high-level features is essential [39, 40]. CNNs have been used in identifying the presence of cracks in butt-fused joints [16] but have been unable to quantify the crack length accurately.

Applying rapidly obtained, unprocessed microseconds of ultrasound time signal to accurately quantify key hidden cracks features in *polymers* has not been done. We present a method that applies fully computational simulations trained CNN to accurately quantify the length and position of penny-shaped embedded cracks in semicrystalline polymer HDPE from reflected ultrasound time signal NDT. It is not feasible to create well-labeled experimental NDT datasets for embedded non-visible cracks [41]. This hampers the application of machine learning for crack quantification in HDPE. To fill this gap, finite element simulations using Abaqus software were developed for HDPE to create training datasets for CNN. A commercial ultrasound test unit was used to obtain A-scan measurements on HDPE specimens containing embedded cracks. The fully computationally trained CNN was applied to the independent experimental signals. The CNN can predict the length and position of embedded elliptical cracks in HDPE samples with good accuracy.

## 2. Computational Method

### 2.1. Finite element simulations for ultrasonic NDT

Finite element simulations were conducted using Abaqus to first evaluate acoustic attenuation and dispersion of the transmitted A-scan ultrasound signals within HDPE specimens and then create a simulation-based training dataset for CNN. Finite element methods have been successfully applied to various engineering applications and proven effective for yielding accurate and reliable results [42, 43, 44, 45, 46, 47]. Assumptions of elasticity for long ultrasound wave propagation distances generally do not hold for HDPE as they do for metals such as steel [29]. Viscoelastic behavior may affect ultrasound signals due to dissipation. By measuring the acoustic attenuation of A-scan ultrasound signals, we can evaluate the extent to which viscoelasticity impacts the characterization of crack length. Initial simulations were conducted for a 12.7 mm thick flat sheet with no crack. HDPE’s material properties were chosen with assumptions of linear elasticity. Young’s modulus was 0.97 GPa, Poisson’s ratio was 0.43, and the density was 954 kg/m<sup>3</sup>. These material properties are typical for HDPE [18]. A calibration experiment was also performed on a 12.7 mm thick flat sheet of HDPE using a 1 MHz transducer on Olympus Epoch 650 Ultrasound NDT equipment (Figure 7). For Natural gas, water and many other pipeline applications, 12.7 mm represents a commonly used pipe thickness. Figure 1 compares the ultrasound signals obtained from the simulation and the calibration experiment. The two peaks represent the first and second back-wall echos. Note that the initial pulse was omitted here, as its amplitude is outside of the ultrasound equipment’s data acquisition limit.

Signal attenuation was determined to be negligible for the 1 MHz frequency and 25.4 mm and 50.8 mm acoustic travel distance in this study. This is evidenced by similar maxima at each peak in both the simulated and experiment ultrasound signals. The width of each echo also indicates insignificant signal dispersion. Therefore, we can conclude that

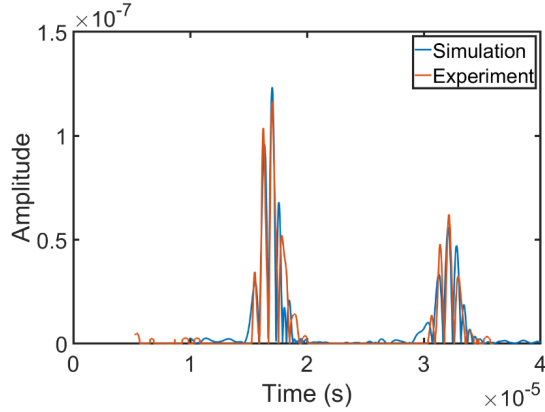


Figure 1: Experimental and simulation ultrasound signals for a 12.7 mm thick flat sheet of HDPE without any cracks.

for small acoustic travel distances and frequencies near 1 MHz, signal attenuation and dispersion negligibly affect the final ultrasound signals. The HDPE response can thus be assumed to be dominantly elastic in this regime. This observation is consistent with linear elastic conclusions in the slow crack growth studies of Chan and Williams [19]. All simulations for this study assumed linear elastic material properties for HDPE.

We consider the crack length and crack position as two main parameters to quantify for embedded cracks in HDPE. We consider a cuboid (block) geometry mimicking a small section of a large span structure or a section of a large radius-to-thickness ratio pipe. The crack is taken to have a penny-shaped, elliptical geometry. The crack length is defined as the major axis of the crack, and the crack position is defined as the distance between the transducer (measurement surface) and the crack. The crack is taken to be oriented horizontally in the plane that has 12.7 mm thickness. The crack’s minor axis was fixed at 0.5 mm, and the crack length varied from 1 to 6 mm. This provides a ratio of crack length to thickness range between 2 and 12. Additionally, the crack position varied between 3 and 11 mm. Evenly dividing the ranges for crack length and crack position into 40 intervals yields a dataset containing  $40 \times 40 = 1600$  simulated ultrasound signals. Table 1 summarizes the crack property ranges used in our finite element simulations, and Figure 2 shows the geometry.

Table 1: Embedded crack length and position range in HDPE considered in this study.

Parameter	Length	Position
Min	1 mm	3 mm
Max	6 mm	11 mm

Next, finite element simulations were performed using Abaqus/Explicit to reproduce ultrasound NDT for HDPE on a computer. The HDPE geometry was defined as a  $40 \times 40 \times 12.7$  mm rectangular cuboid. The ultrasonic signal propagation was directed in the 12.7 mm thickness dimension, with a frequency of 1 MHz and 2.5 mm wavelength.

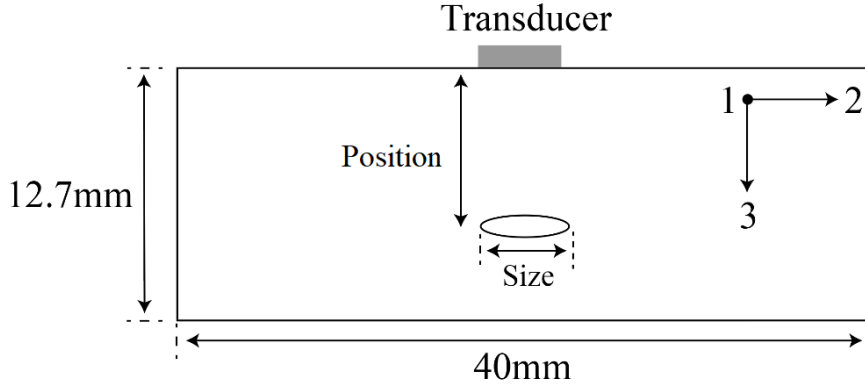


Figure 2: Cross-sectional view illustrating two key crack properties of the HDPE block on its symmetry plane. These properties are the crack length  $a$  and the crack position  $d$ .

Since this cuboid is symmetrical, only half of it was simulated. The center of the simulated geometry contains an embedded flaw. Because the speed of sound in HDPE is rather fast (2340 m/s), the element sizes need to be sufficiently small to ensure numerical stability. Thus a very fine mesh with an element size of 0.1 mm was used near the flaw, with the element size gradually increasing in the domain far from the flaw. Since the geometry near the flaw is irregular, the central region containing the flaw was meshed using C3D10M tetrahedral elements. The remainder of the geometry utilized C3D8R brick elements to improve computational efficiency away from the flaw. Figure 3(a) depicts the cross-section for a typical mesh used with this geometry. The total number of elements in each finite element simulation was between three and four hundred thousand. The total simulation time was 20 microseconds, and the time step was fixed at 10 nanoseconds. Consistent with the transducer size available for experiments, a time-dependent pressure boundary condition was employed on a 12.7 mm diameter circular region. The ultrasound pulse was simulated with a raised-cosine type waveform at 1 MHz frequency, as shown in figure 3(b). The period of the signal is  $2.5 \mu\text{s}$ , and the longitudinal wave travels in the 12.7 mm thickness direction.

## 2.2. Simulation trained convolutional neural network

The CNN is a feed forward neural network with an efficient architecture ideal for applications in imaging, speech and signal processing, and more. CNN and other machine learning techniques are also becoming increasingly useful for structural mechanics problems. Machine learning has been used to solve physics-informed partial differential equations [48], model fluid flow [49], predicting mechanical properties with continuum mechanics approach [50, 51], and ascertaining constitutive properties [52]. 2D image-based CNNs have been used to discern properties of surface cracks from ultrasonic images of the cracks [53]. CNNs can also process noisy ultrasound signals with high accuracy for the classification of weldment flaw defects [54]. Krokos et al. [55] applied a Bayesian multiscale CNN to reduce computational costs for modeling structures with microscale

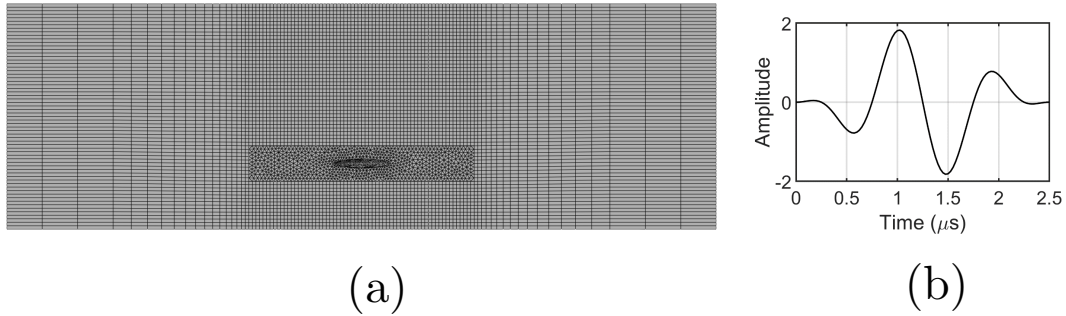


Figure 3: (a) Cross-sectional view showing the finite element mesh of the block on its symmetry plane. The mesh becomes significantly finer as it approaches the central region containing the elliptical flaw. (b) Amplitude versus time plot of the simulated pulse generated by the time-dependent pressure boundary condition at the top surface nodes representing the 12.7 mm diameter circular probe region on the block.

features. Evaluation of the degree of structural damage was studied using echo state networks, and multi-scale CNN [56]. Meng et al. [57] have proposed an automatic ultrasonic signal classification system using a deep neural network for defective carbon fiber composite systems.

A typical CNN architecture consists of three layers: the convolutional layer, the pooling layer, and the fully connected (FC) layer [58]. Inputs are passed first to the convolutional layer, where a kernel or multi-channel filter obtains high-level information (feature extraction). The features are down-sampled in the pooling layer in order to reduce dimensions. Learning occurs in the FC layer, where all the neurons are connected. Assigning an activation function to each neuron in the convolutional and FC layers allows for nonlinear learnability from extracted features [59]. The ReLu activation function is one common choice and was selected for this study due to its fast convergence in CNNs, and notably great performance in deep learning applications [60, 61].

$$\text{ReLu}(z) = \max(0, z) \quad (3)$$

The type of pooling layer also needs to be selected. The max-pooling layer selects local maxima among input features to speed up training and reduce dimensions. Our architecture utilizes a max-pooling layer. Dropout is a technique used to prevent network overfitting [62], in which some neurons within a layer have a probability  $p$  to be deactivated during training. Dropout is effective in regularizing and providing better generalization ability to the network. We have applied dropout to the FC layer. The CNN architecture used in this study (Figure 4) consists of two convolutional layers, one pooling layer, and two FC layers, including the output layer. We have used ReLu in both convolutional layers and the first FC layer. The optimization algorithm utilized was

Adam, and a dropout probability of 0.2 was used in the first FC layer. The mean squared error (MSE) loss function, shown below, was selected as our loss function. Finally, this CNN was trained for 2000 epochs using a learning rate of 0.0005. Table 2 describes the configuration of our CNN in more detail.

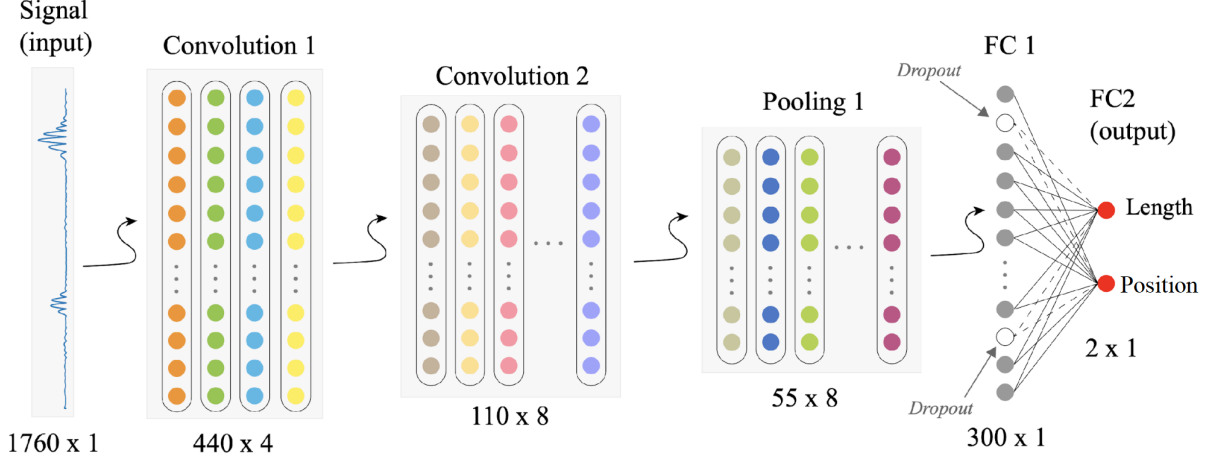


Figure 4: CNN architecture for quantification of embedded crack length and position in HDPE from ultrasound A-scan signals.

$$\text{Loss}_{\text{MSE}} = \sum_{i=1}^n (y_i - t_i)^2 \quad (4)$$

where  $y_i$ : predicted value

$t_i$ : actual/target value

$\text{Loss}_{\text{MSE}}$ : summation of all training data

Table 2: CNN configuration for quantification of embedded crack length and position in HDPE.

Layer type	Channel	Kernel Size	Stride	Padding	Size / Neuron
Convolutional 1	4	8	4	2	440 x 4
Convolutional 2	8	8	4	2	110 x 8
Pooling 1	8	2	2	0	55 x 8
FC 1	-	-	-	-	300
FC 2	-	-	-	-	2

### 2.3. CNN performance on simulations-generated testing signals

An additional 100 finite element simulated signals were generated as part of our simulation-based testing dataset. These signals were not passed to the CNN during training. Crack lengths and positions for this dataset were randomly chosen from the



ranges introduced in Table 1. Figure 5 and Table 3 describe the predictive performance of trained CNN on the simulation-generated independent testing dataset. The x-axis in Figure 5 denotes the actual values of the crack feature in the simulated geometry, and the y-axis denotes predicted values from the CNN. The dashed, black  $45^\circ$  lines represent perfect predictions. The trained CNN demonstrates high accuracy for both crack length and position when provided independent finite element simulated testing data. The mean absolute percent errors (MAPE) of crack length and position are 3.2% and 2.5%, respectively, and the mean absolute errors (MAE) for length and position are 0.05 mm and 0.15 mm. These error values for the simulation testing data are small, indicating the CNN performed well.

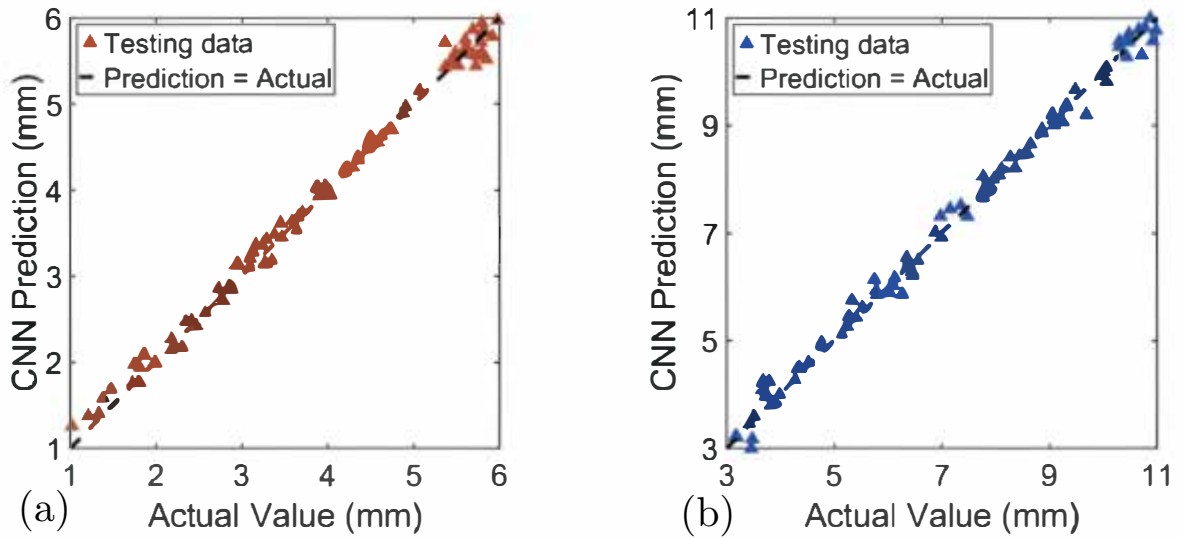


Figure 5: Performance of CNN on simulations generated testing data. Performance on crack length (left) and crack position (right). Points closer to the  $45^\circ$  line indicate higher accuracy predictions.

Table 3: MAPE and MAE of CNN predictions on 100 simulated testing signals

Parameter	MAPE (%)	MAE (mm)
Length	3.2	0.05
Position	2.5	0.15

### 3. Validation Ultrasound Non-Destructive Experiments

#### 3.1. Experimental setup

Independent experimental validation of simulation-trained CNN is important for confirming the accuracy of our finite element simulations trained CNN method for predicting crack characteristics within real HDPE samples. We performed ultrasound NDT tests on fabricated HDPE specimens and applied previously simulation-trained CNN to predict the crack lengths and positions in HDPE test specimens. Test samples with embedded,

non-visible cracks can be fabricated by 3D printing technology [30]. Compared to the conventionally processed bulk HDPE used in structural applications, 3D printed polymeric specimens would have significantly different attributes. HDPE experiences shrinking, voiding, and warping once extruded in this method [63]. Additionally, the resulting 3D printed polymeric structure is highly porous. The high porosity of the structure can negatively affect ultrasound wave propagation and acoustic transmission. Since we are primarily focused on conventionally processed HDPE, we developed a test specimen fabrication method that did not rely on 3D printing.

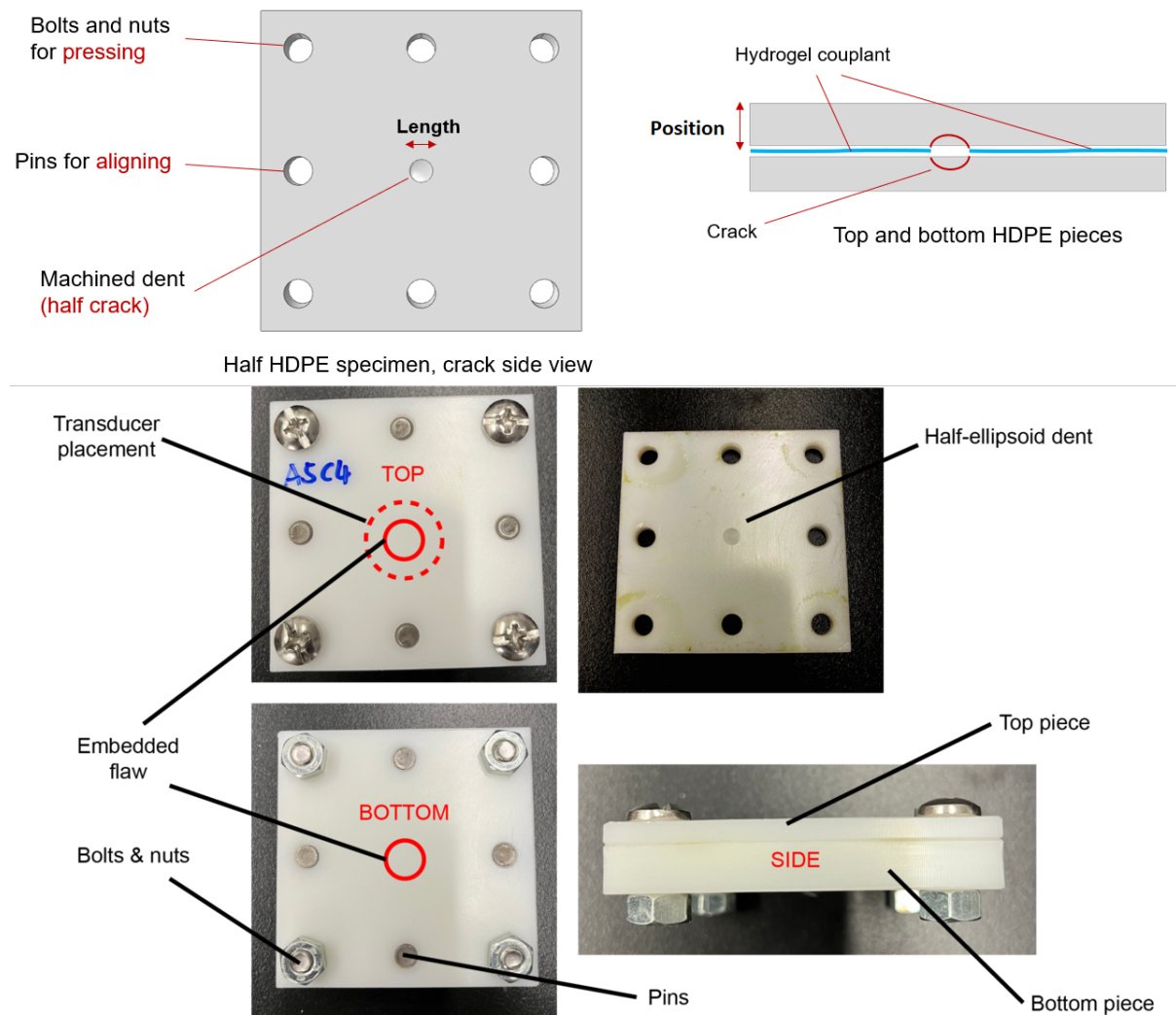


Figure 6: The experimental design for HDPE specimen with an embedded crack (top) and one of the fabricated HDPE specimens for ultrasound testing following the design procedure (below).

Our design for HDPE specimens with embedded cracks is illustrated in Figure 6. Every test specimen was constructed using two flat sheets of HDPE, each with an in-plane length and width of 70 mm and varying thicknesses. The thickness of the two sheets were individually varied to change the through thickness crack position while keeping the overall specimen thickness at 12.7 mm. A half-ellipsoid dent was machined

in the center of each sheet. Pressing the two sheets together with the dents facing each other results in an elliptical penny-shaped gap invisible from the exterior. This penny-shaped void serves to represent a non-visible, embedded crack. To ensure the two sheets were aligned once pressed together, eight 6.25 mm diameter holes were machined on the four edges and four corners. The corner holes served to hold tightly screwed bolts for the purpose of pressing and securing the two sheets together, while the edge holes held metal dowel pins to maintain alignment. The large  $70 \times 70$  mm size and the dowel and bolt locations were chosen to keep waves reflected from the dowels, bolts and side boundaries outside the window of through thickness reflected wave measurements. These specimens and measurements represent through thickness measurements of embedded cracks in structures with large transverse spans (e.g., pipelines, storage tanks, etc.). To avoid potential air gaps in the mating surfaces, hydrogel couplant (35% propylene glycol) was applied between the top and bottom sheets, then they were tightly pressed together<sup>1</sup>. The crack size and position were varied across fifteen fabricated HDPE specimens. The crack lengths selected were 2, 3, 4, 5, and 6 mm, and the crack positions were chosen to be 4, 7, and 10 mm from the surface of the specimen. Each specimen can be tested from both sides, resulting in thirty possible experiments. Five cases with very shallow crack positions (2.7 mm) were not considered because the crack echo and initial sensor pulse could overlap and interfere in these cases. Removing these five experimental signals yields a final count of 25 independent experimental signals. All ultrasound experiments were conducted using an Olympus Epoch 650 Ultrasound NDT Flaw Detector, seen in Figure 7. The transducer used was a straight beam and single element with a frequency of 1 MHz and a sensor surface diameter of 12.7 mm.



Figure 7: The Olympus Epoch 650 Ultrasound NDT Flaw Detector used in this study (left). The transducer has a 12.7 mm diameter and is a straight beam single element transducer (right).

---

<sup>1</sup>The sheets were separated to observe if any couplant was smeared into the crack. Any smeared couplant was removed from the crack indentation, and the process was repeated again until no gel was visible inside the crack.

### 3.2. Experimental results

The finite element trained CNN was applied to twenty-five ultrasound signals obtained from NDT of the fabricated HDPE specimens with varying embedded crack lengths and positions. No experimental data was used to train the CNN, and these experiments were conducted solely to validate the proposed methodology for HDPE.

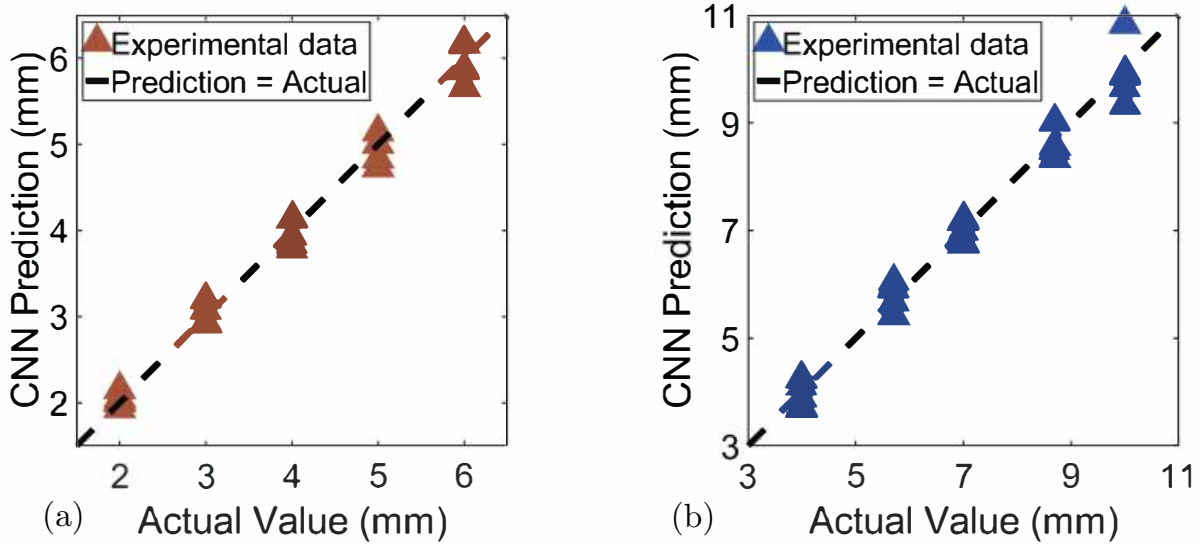


Figure 8: CNN performance on ultrasound NDT experimental data. CNN predictive performance for (a) crack length and (b) crack position. Points closer to the 45° line indicate higher accuracy predictions.

Figure 8 presents the results of the CNN on the experimental signals. The 45° line represents a perfect fit. Points close to the line indicate the high accuracy of the predictions. These results demonstrate that the CNN is accurately predicting both crack length and crack position simultaneously from experimental ultrasound signals. Table 4 lists the CNN predictions, true values, and percentage errors for the two crack characteristics. The mean absolute percent error (MAPE) was found to be 3.24% for length and 3.78% for position. The mean absolute error (MAE) for length and position was 0.07 and 0.26 mm, respectively.

## 4. Conclusions

Flaws can manifest in polymers during fabrication or operations. As the demand for polymers increases, so does the need for rapid and accurate characterization of crack length and position to avoid sudden catastrophic failures. Processing and interpreting ultrasound signals using machine learning techniques have demonstrated significant potential, especially for detecting non-visible, embedded flaws. Machine learning has been applied to image based ultrasound applications. Our finite element trained CNN method for HDPE is based on ultrasound time amplitude signal and not based on image analysis. This is an important distinction as the 2D image rendering NDT process is very slow and is limited as it is susceptible to losing subtle crack features information during the

Table 4: Detailed summary of simulation-trained CNN performance on experimental ultrasound measurements on HDPE.

Specimen Number	Length (mm)			Position (mm)		
	Actual	Predicted	Error	Actual	Predicted	Error
1	2	2.15	7.72%	4	3.69	7.82%
2	2	2.05	2.52%	5.7	5.41	5.11%
3	2	1.93	3.39%	7	6.79	2.95%
4	2	2.02	0.98%	8.7	9.02	3.68%
5	2	2	0.04%	10	9.65	3.48%
6	3	3.07	2.46%	4	3.73	6.77%
7	3	2.93	2.24%	5.7	5.66	0.73%
8	3	2.94	1.93%	7	7.16	2.35%
9	3	2.92	2.80%	8.7	8.33	4.20%
10	3	3.19	6.41%	10	10.84	8.36%
11	4	4.14	3.44%	4	3.88	3%
12	4	3.84	3.93%	5.7	5.9	3.53%
13	4	3.93	1.64%	7	6.74	3.71%
14	4	3.78	5.46%	8.7	8.34	4.15%
15	4	4.14	3.54%	10	9.86	1.35%
16	5	4.83	3.34%	4	4.23	5.78%
17	5	4.73	5.31%	5.7	6.05	6.12%
18	5	4.73	5.40%	7	7.21	3.03%
19	5	5.15	2.90%	8.7	8.56	1.57%
20	5	5	0.07%	10	9.93	0.75%
21	6	5.67	5.57%	4	4.1	2.45%
22	6	5.89	1.83%	5.7	5.93	3.99%
23	6	6.16	2.69%	7	6.98	0.27%
24	6	6.18	2.97%	8.7	8.48	2.51%
25	6	5.86	2.36%	10	9.32	6.75%
MAPE	3.24%			3.78%		
MAE	0.07 mm			0.26 mm		

post-processing required to create images. The ultrasound time signal data with measurement windows of tens of microseconds at each location is convenient for measuring in large structures. Our study confirms that acoustic attenuation and dispersion due to viscoelasticity in HDPE can be reasonably neglected for 1 MHz frequency and relatively shorter signal travel distances ( $\sim 50$  mm). We conducted 3D finite element simulations representing ultrasonic A-scan wave propagation inside HDPE with embedded cracks to show that simulation-generated ultrasound signals can train signal-based CNN well. We demonstrate that the simulation-trained CNN can subsequently predict the crack length

and position of penny-shaped embedded cracks in real HDPE samples with very good accuracy. In our study, the average error in crack length and position predictions was less than 3.8%. As summarized in Figure 9, this study suggests a method for HDPE that can potentially be extended to other solid polymers where a CNN is trained using geometry and flaw type specific finite element ultrasound wave propagation simulations and then applied onboard an inspection tool to detect and characterize the specific flaws that it is trained for.

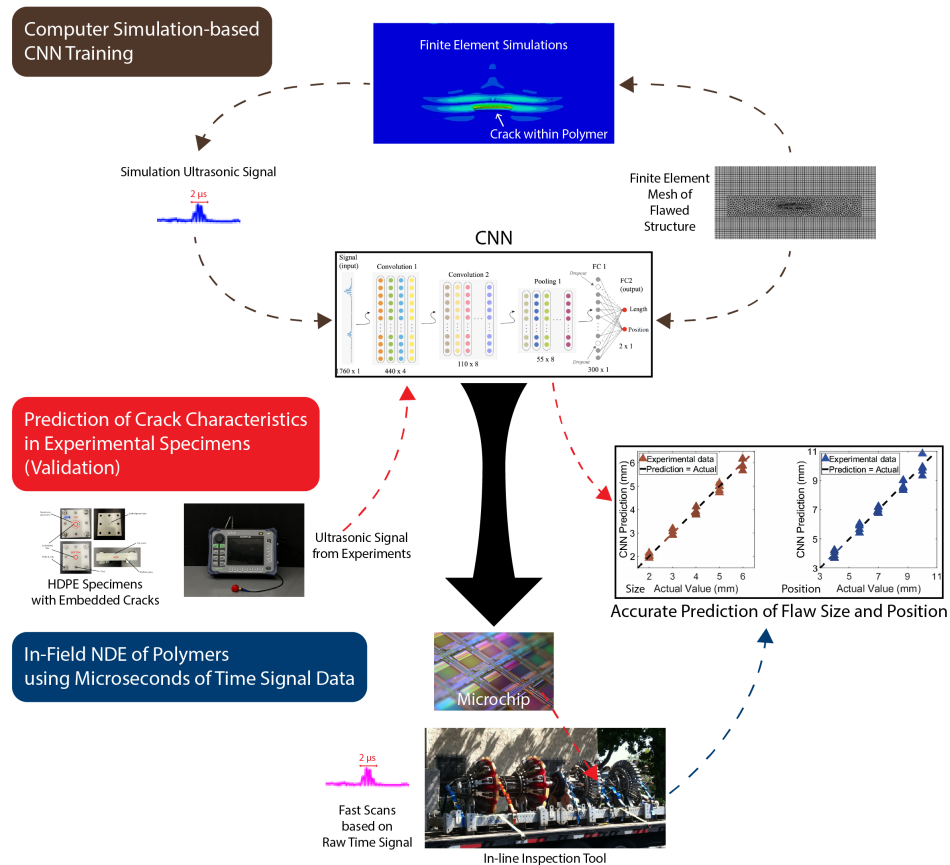


Figure 9: NDE method for crack measurements from microseconds of ultrasound time signal and its potential application in structures like long pipelines using In-Line-Inspection (ILI) devices. Images with permission from [64, 65]

## Declaration of Competing Interest

The authors declare no conflict of interest.

## Data Availability

The data will be available upon request.

## Acknowledgement

We gratefully acknowledge support from the U.S. Department of Transportation to V. Srivastava under grant number 693JK32050001CAAP. The views and opinions expressed in this article are those of the authors and do not necessarily reflect the official policy or position of any agency of the U.S. government.

## References

- [1] M. Demirors, The history of polyethylene, in: 100+ Years of Plastics. Leo Baekeland and Beyond, ACS Publications, 2011, pp. 115–145. doi:10.1021/bk-2011-1080.ch009.
- [2] N. C. Paxton, M. C. Allenby, P. M. Lewis, M. A. Woodruff, Biomedical applications of polyethylene, *European Polymer Journal* 118 (2019) 412–428. doi:10.1016/j.eurpolymj.2019.05.037.
- [3] H. Fouad, R. Elleithy, O. Y. Alothman, Thermo-mechanical, Wear and Fracture Behavior of High-density Polyethylene/Hydroxyapatite Nano Composite for Biomedical Applications: Effect of Accelerated Ageing, *Journal of Materials Science & Technology* 29 (6) (2013) 573–581. doi:10.1016/j.jmst.2013.03.020.
- [4] S. Stuart, Evaluation of HDPE and PVC pipes used for cross-drains in highway construction, Ph.D. thesis, Auburn University (2011).
- [5] J. Goddard, Growth of thermoplastic pipe use in transportation applications, *Culverts and Soil-Structure Interaction* (2018) 34.
- [6] Y. Gong, S.-H. Wang, Z.-Y. Zhang, X.-L. Yang, Z.-G. Yang, H.-G. Yang, Degradation of sunlight exposure on the high-density polyethylene (hdpe) pipes for transportation of natural gases, *Polymer Degradation and Stability* 194 (2021) 109752. doi:https://doi.org/10.1016/j.polymdegradstab.2021.109752.
- [7] A. Tutunchi, M. Eskandarzade, K. Osouli-Bostanabad, R. Shahrivar, Risk assessment of an urban natural gas polyethylene piping system, *Journal of Pipeline Systems Engineering and Practice* 11 (2) (2020) 06019005. doi:10.1061/(ASCE)PS.1949-1204.0000440.
- [8] T. Bachir-Bey, N. Belhaneche-Bensemra, Investigation of polyethylene pipeline behavior after 30 years of use in gas distribution network, *Journal of Materials Engineering and Performance* 29 (10) (2020) 6652–6660. doi:10.1007/s11665-020-05118-9.

- [9] J. Zheng, Y. Zhang, D. Hou, Y. Qin, W. Guo, C. Zhang, J. Shi, A review of nondestructive examination technology for polyethylene pipe in nuclear power plant, *Frontiers of Mechanical Engineering* 13 (4) (2018) 535–545. doi:10.1007/s11465-018-0515-9.
- [10] H. Iskov, H. D. Danish Gas Technology Centre, Field test of hydrogen in the natural gas grid, Project Report.
- [11] K. Q. Nguyen, C. Mwiseneza, K. Mohamed, P. Cousin, M. Robert, B. Benmokrane, Long-term testing methods for HDPE pipe - advantages and disadvantages: A review, *Engineering Fracture Mechanics* 246 (2021) 107629. doi:10.1016/j.engfracmech.2021.107629.
- [12] R. W. Lang, A. Stern, G. Doerner, Applicability and limitations of current lifetime prediction models for thermoplastics pipes under internal pressure, *Die Angewandte Makromolekulare Chemie: Applied Macromolecular Chemistry and Physics* 247 (1) (1997) 131–145. doi:10.1002/apmc.1997.052470109.
- [13] H. H. Kausch, The nature of defects and their role in large deformation and fracture of engineering thermoplastics, *Pure and Applied Chemistry* 55 (5) (1983) 833–844. doi:10.1351/pac198355050833.
- [14] S. Gassman, A. Schroeder, R. Ray, Field Performance of High Density Polyethylene Culvert Pipe, *Journal of Transportation Engineering-asce - J TRANSP ENG-ASCE* 131. doi:10.1061/(ASCE)0733-947X(2005)131:2(160).
- [15] R. Schouwenaars, V. Jacobo, E. Ramos, A. Ortiz, Slow crack growth and failure induced by manufacturing defects in HDPE-tubes, *Engineering Failure Analysis* 14 (6) (2007) 1124–1134. doi:10.1016/j.engfailanal.2006.11.066.
- [16] M. Shafiei Alavijeh, R. Scott, F. Seviaryn, R. G. Maev, Using machine learning to automate ultrasound-based classification of butt-fused joints in medium-density polyethylene gas pipes, *The Journal of the Acoustical Society of America* 150 (1) (2021) 561–572. doi:10.1121/10.0005656.
- [17] R. Schouwenaars, V. Jacobo, E. Ramos, A. Ortiz, Slow crack growth and failure induced by manufacturing defects in hdpe-tubes, *Engineering Failure Analysis* 14 (6) (2007) 1124–1134. doi:https://doi.org/10.1016/j.engfailanal.2006.11.066.
- [18] N. Brown, X. Lu, A fundamental theory for slow crack growth in polyethylene, *Polymer* 36 (3) (1995) 543–548. doi:10.1016/0032-3861(95)91563-M.
- [19] M. K. V. Chan, J. G. Williams, Slow stable crack growth in high density polyethylenes, *Polymer* 24 (2) (1983) 234–244. doi:https://doi.org/10.1016/0032-3861(83)90139-8.



- [20] M. Troughton, A comparison of mechanical test methods for butt fusion joints in polyethylene pipes, 2010 NACE northern area western conference.
- [21] A. Behravan, T. Q. Tran, Y. Li, M. Davis, M. S. Shaikh, M. M. DeJong, A. Hernandez, A. S. Brand, Field Inspection of High-Density Polyethylene (HDPE) Storage Tanks Using Infrared Thermography and Ultrasonic Methods, *Applied Sciences* 13 (3) (2023) 1396. doi:10.3390/app13031396.
- [22] S. L. Crawford, S. R. Doctor, A. D. Cinson, M. W. Watts, T. L. Moran, M. T. Anderson, Preliminary Assessment of NDE Methods on Inspection of HDPE Butt Fusion Piping Joints for Lack of Fusion With Validation From Mechanical Testing, in: *ASME 2010 Pressure Vessels and Piping Conference: Volume 6, Parts A and B*, ASME, 2010, pp. 1039–1045. doi:10.1115/PVP2010-25280.
- [23] R. Stakenborghs, J. Little, Microwave Based NDE Inspection of HDPE Pipe Welds, in: *Volume 4: Codes, Standards, Licensing and Regulatory Issues; Student Paper Competition*, ASME, 2009, pp. 185–193. doi:10.1115/ICONE17-75742.
- [24] Y. Yao, S.-T. E. Tung, B. Glisic, Crack detection and characterization techniques—An overview, *Structural Control and Health Monitoring* 21 (12) (2014) 1387–1413. doi:10.1002/stc.1655.
- [25] P. J. Postma, R. J. M. Hermkens, Suitability of non destructive techniques for testing polyethylene pipe joints, *Plastic Pipes XVI* (2012) 1–10.
- [26] J. Zhu, R. P. Collins, J. B. Boxall, R. S. Mills, R. Dwyer-joyce, Non-Destructive In-Situ Condition Assessment of Plastic Pipe Using Ultrasound, *Procedia Engineering* 119 (2015) 148–157. doi:10.1016/j.proeng.2015.08.866.
- [27] C. Frederick, A. Porter, D. Zimmerman, High-Density Polyethylene Piping Butt-Fusion Joint Examination Using Ultrasonic Phased Array, *Journal of Pressure Vessel Technology* 132 (5). doi:10.1115/1.4001212.
- [28] A. Oishi, K. Yamada, S. Yoshimura, G. Yagawa, S. Nagai, Y. Matsuda, Neural network-based inverse analysis for defect identification with laser ultrasonics, *Research in nondestructive evaluation* 13 (2) (2001) 79–96. doi:10.1007/s00164-001-0010-1.
- [29] S. Niu, V. Srivastava, Ultrasound classification of interacting flaws using finite element simulations and convolutional neural network, *Engineering with Computers* 38 (5) (2022) 4653–4662. doi:10.1007/s00366-022-01681-y.
- [30] S. Niu, V. Srivastava, Simulation trained CNN for accurate embedded crack length, location, and orientation prediction from ultrasound measurements, *International*

- Journal of Solids and Structures 242 (2022) 111521. doi:10.1016/j.ijsolstr.2022.111521.
- [31] W. Liu, Z. Wang, X. Liu, N. Zeng, Y. Liu, F. E. Alsaadi, A survey of deep neural network architectures and their applications, *Neurocomputing* 234 (2017) 11–26. doi:10.1016/j.neucom.2016.12.038.
- [32] F. E. Bock, R. C. Aydin, C. J. Cyron, N. Huber, S. R. Kalidindi, B. Klusemann, A Review of the Application of Machine Learning and Data Mining Approaches in Continuum Materials Mechanics, *Frontiers in Materials* 6 (2019) 110. doi:10.3389/fmats.2019.00110.
- [33] S. Niu, E. Zhang, Y. Bazilevs, V. Srivastava, Modeling finite-strain plasticity using physics-informed neural network and assessment of the network performance, *Journal of the Mechanics and Physics of Solids* 172 (2023) 105177. doi:10.1016/J.JMPS.2022.105177.
- [34] K. Linka, S. R. St. Pierre, E. Kuhl, Automated model discovery for human brain using constitutive artificial neural networks, *Acta Biomaterialia* 160 (2023) 134–151. doi:https://doi.org/10.1016/j.actbio.2023.01.055.
- [35] K. Linka, E. Kuhl, A new family of constitutive artificial neural networks towards automated model discovery, *Computer Methods in Applied Mechanics and Engineering* 403 (2023) 115731. doi:https://doi.org/10.1016/j.cma.2022.115731.
- [36] Y.-C. Hsu, C.-H. Yu, M. J. Buehler, Using Deep Learning to Predict Fracture Patterns in Crystalline Solids, *Matter* 3 (1) (2020) 197–211. doi:10.1016/j.matt.2020.04.019.
- [37] Q. Wang, X. Zhuang, A cnn-based surrogate model of isogeometric analysis in non-local flexoelectric problems, *Engineering with Computers* 39 (1) (2023) 943–958. doi:10.1007/s00366-022-01717-3.
- [38] C. L. Chan, F. Scholz, T. Takacs, Locally refined quad meshing for linear elasticity problems based on convolutional neural networks, *Engineering with Computers* 38 (5) (2022) 4631–4652. doi:10.1007/s00366-022-01677-8.
- [39] Y. LeCun, Y. Bengio, G. Hinton, Deep learning, *Nature* 521 (7553) (2015) 436–444. doi:10.1038/nature14539.
- [40] M. D. Zeiler, R. Fergus, Visualizing and Understanding Convolutional Networks, *Computer Vision – ECCV 2014, Lecture Notes in Computer Science* (2014) 818–833doi:10.1007/978-3-319-10590-1\_{\\_}53.

- [41] S. Cantero-Chinchilla, P. D. Wilcox, A. J. Croxford, Deep learning in automated ultrasonic nde – developments, axioms and opportunities, *NDT & E International* 131 (2022) 102703. doi:<https://doi.org/10.1016/j.ndteint.2022.102703>.
- [42] A. Konale, Z. Ahmed, P. Wanchoo, V. Srivastava, A large deformation model for quasi-static to high strain rate response of a rate-stiffening soft polymer, *International Journal of Plasticity* 168 (2023) 103701. doi:<https://doi.org/10.1016/j.ijplas.2023.103701>.
- [43] V. Srivastava, S. A. Chester, L. Anand, Thermally actuated shape-memory polymers: Experiments, theory, and numerical simulations, *Journal of the Mechanics and Physics of Solids* 58 (8) (2010) 1100–1124. doi:[10.1016/j.jmps.2010.04.004](https://doi.org/10.1016/j.jmps.2010.04.004).
- [44] Y. Bai, N. J. Kaiser, K. L. Coulombe, V. Srivastava, A continuum model and simulations for large deformation of anisotropic fiber–matrix composites for cardiac tissue engineering, *Journal of the Mechanical Behavior of Biomedical Materials* 121 (2021) 104627. doi:[10.1016/j.jmbbm.2021.104627](https://doi.org/10.1016/j.jmbbm.2021.104627).
- [45] J. Zhong, V. Srivastava, A higher-order morphoelastic beam model for tubes and filaments subjected to biological growth, *International Journal of Solids and Structures* 233 (2021) 111235. doi:[10.1016/j.ijsolstr.2021.111235](https://doi.org/10.1016/j.ijsolstr.2021.111235).
- [46] M. Kothari, S. Niu, V. Srivastava, A thermo-mechanically coupled finite strain model for phase-transitioning austenitic steels in ambient to cryogenic temperature range, *Journal of the Mechanics and Physics of Solids* 133 (2019) 103729. doi:[10.1016/j.jmps.2019.103729](https://doi.org/10.1016/j.jmps.2019.103729).
- [47] V. Srivastava, J. Buitrago, S. T. Slocum, Stress analysis of a cryogenic corrugated pipe, in: *Proceedings of the ASME 2011 30th International Conference on Ocean, Offshore and Arctic Engineering: Volume 3*, American Society of Mechanical Engineers, 2011, pp. 411–422. doi:[10.1115/OMAE2011-49852](https://doi.org/10.1115/OMAE2011-49852).
- [48] M. Raissi, P. Perdikaris, G. E. Karniadakis, Physics-informed neural networks: A deep learning framework for solving forward and inverse problems involving nonlinear partial differential equations, *Journal of Computational Physics* 378 (2019) 686–707. doi:[10.1016/J.JCP.2018.10.045](https://doi.org/10.1016/J.JCP.2018.10.045).
- [49] S. L. Brunton, B. R. Noack, P. Koumoutsakos, Machine Learning for Fluid Mechanics, <https://doi.org/10.1146/annurev-fluid-010719-060214> 52 (2020) 477–508. doi:[10.1146/ANNUREV-FLUID-010719-060214](https://doi.org/10.1146/ANNUREV-FLUID-010719-060214).
- [50] L. Lu, M. Dao, P. Kumar, U. Ramamurty, G. E. Karniadakis, S. Suresh, Extraction of mechanical properties of materials through deep learning from instrumented indentation, *Proceedings of the National Academy of Sciences of the United States*

- of America 117 (13) (2020) 7052–7062. doi:10.1073/PNAS.1922210117/SUPPL{\\_}FILE/PNAS.1922210117.SAPP.PDF.
- [51] X. Li, Z. Liu, S. Cui, C. Luo, C. Li, Z. Zhuang, Predicting the effective mechanical property of heterogeneous materials by image based modeling and deep learning, *Computer Methods in Applied Mechanics and Engineering* 347 (2019) 735–753. doi:10.1016/J.CMA.2019.01.005.
- [52] N. Huber, S. R. Kalidindi, B. Klusemann, C. J. Cyron, Editorial: Machine Learning and Data Mining in Materials Science, *Frontiers in Materials* 7 (2020) 51. doi:10.3389/FMATS.2020.00051/BIBTEX.
- [53] R. J. Pyle, R. L. Bevan, R. R. Hughes, R. K. Rachev, A. A. S. Ali, P. D. Wilcox, Deep Learning for Ultrasonic Crack Characterization in NDE, *IEEE Transactions on Ultrasonics, Ferroelectrics, and Frequency Control* 68 (5) (2021) 1854–1865. doi:10.1109/TUFFC.2020.3045847.
- [54] N. Munir, H. J. Kim, J. Park, S. J. Song, S. S. Kang, Convolutional neural network for ultrasonic weldment flaw classification in noisy conditions, *Ultrasonics* 94 (2019) 74–81. doi:10.1016/J.ULTRAS.2018.12.001.
- [55] V. Krokos, V. Bui Xuan, S. P. Bordas, P. Young, P. Kerfriden, A Bayesian multiscale CNN framework to predict local stress fields in structures with microscale features, *Computational Mechanics* 69 (3) (2022) 733–766. doi:10.1007/S00466-021-02112-3/FIGURES/42.
- [56] Y. He, L. Zhang, Z. Chen, C. Y. Li, A framework of structural damage detection for civil structures using a combined multi-scale convolutional neural network and echo state network, *Engineering with Computers* doi:10.1007/s00366-021-01584-4.
- [57] M. Meng, Y. J. Chua, E. Wouterson, C. P. K. Ong, Ultrasonic signal classification and imaging system for composite materials via deep convolutional neural networks, *Neurocomputing* 257 (2017) 128–135. doi:10.1016/J.NEUCOM.2016.11.066.
- [58] L. Wen, X. Li, L. Gao, Y. Zhang, A New Convolutional Neural Network-Based Data-Driven Fault Diagnosis Method, *IEEE Transactions on Industrial Electronics* 65 (7) (2018) 5990–5998. doi:10.1109/TIE.2017.2774777.
- [59] W. Zhang, C. Li, G. Peng, Y. Chen, Z. Zhang, A deep convolutional neural network with new training methods for bearing fault diagnosis under noisy environment and different working load, *Mechanical Systems and Signal Processing* 100 (2018) 439–453. doi:10.1016/j.ymssp.2017.06.022.
- [60] A. L. Maas, A. Y. Hannun, A. Y. Ng, others, Rectifier nonlinearities improve neural network acoustic models, in: *Proc. icml*, Vol. 30, 2013, p. 3.

- [61] V. Nair, G. E. Hinton, Rectified linear units improve restricted boltzmann machines, in: Proceedings of the 27th international conference on machine learning (ICML-10), 2010, pp. 807–814.
- [62] N. Srivastava, G. Hinton, A. Krizhevsky, I. Sutskever, R. Salakhutdinov, Dropout: A Simple Way to Prevent Neural Networks from Overfitting, *J. Mach. Learn. Res.* 15 (1) (2014) 1929–1958.
- [63] C. G. Schirmeister, T. Hees, E. H. Licht, R. Mülhaupt, 3D printing of high density polyethylene by fused filament fabrication, *Additive Manufacturing* 28 (2019) 152–159. doi:10.1016/j.addma.2019.05.003.
- [64] L. Ockel, Web micro chip image, Licensed under CC BY-SA 4.0.doi:<https://unsplash.com/photos/pink-green-and-blue-square-pattern-q0x9KsvpqcM>.
- [65] Lemonn, Web ili tool image, Licensed under CC BY-SA 4.0.doi:[https://commons.wikimedia.org/wiki/File:Smart\\\_pig.jpg](https://commons.wikimedia.org/wiki/File:Smart\_pig.jpg).